Isomer depletion as experimental evidence of nuclear excitation by electron capture

C. J. Chiara[1], J. J. Carroll[2], M. P. Carpenter[3], J. P. Greene[3], D. J. Hartley[4], R. V. F. Janssens[3]†, G. J. Lane[5], J. C. Marsh[1]†, D. A. Matters[6], M. Polasik[7], J. Rzadkiewicz[8], D. Seweryniak[3], S. Zhu[3], S. Bottoni[3]†, A. B. Hayes[9] & S. A. Karamian[10]‡

The atomic nucleus and its electrons are often thought of as independent systems that are held together in the atom by their mutual attraction. Their interaction, however, leads to other important effects, such as providing an additional decay mode for excited nuclear states, whereby the nucleus releases energy by ejecting an atomic electron instead of by emitting a γ-ray. This 'internal conversion' has been known for about a hundred years and can be used to study nuclei and their interaction with their electrons[1–3]. In the inverse process—nuclear excitation by electron capture (NEEC)—a free electron is captured into an atomic vacancy and can excite the nucleus to a higher-energy state, provided that the kinetic energy of the free electron plus the magnitude of its binding energy once captured matches the nuclear energy difference between the two states. NEEC was predicted[4] in 1976 and has not hitherto been observed[5,6]. Here we report evidence of NEEC in molybdenum-93 and determine the probability and cross-section for the process in a beam-based experimental scenario. Our results provide a standard for the assessment of theoretical models relevant to NEEC, which predict cross-sections that span many orders of magnitude. The greatest practical effect of the NEEC process may be on the survival of nuclei in stellar environments[7], in which it could excite isomers (that is, long-lived nuclear states) to shorter-lived states. Such excitations may reduce the abundance of the isotope after its production. This is an example of 'isomer depletion', which has been investigated previously through other reactions[8–12], but is used here to obtain evidence for NEEC.

We searched for evidence of the NEEC process in ^{93}Mo following an approach adapted from a technique proposed in ref. 13. Previous theoretical work also considered ^{93}Mo as a NEEC candidate[6]. This nucleus has a $21/2^+$ isomer at 2,425 keV with a half-life of 6.85 h and a $(17/2)^+$ candidate intermediate state that lies 4.85(9) keV higher at 2,430 keV (ref. 14), as illustrated in Fig. 1. (Uncertainties are quoted at the 1σ or 68% confidence level, unless otherwise noted.) In our approach, ^{93}Mo is produced in its metastable state (^{93m}Mo) through nuclear reactions. Choosing heavy projectiles and light target nuclei results in recoiling ^{93m}Mo reaction products ('recoils') that move at high velocities v (initially more than 10% of the speed of light, c) in approximately the same direction as the beam. As the fast-moving recoils pass through the target medium, electrons are stripped off, leaving the ^{93m}Mo ions with a high average charge[15,16] between about +32 and +36. Subsequent collisions with target atoms reduce the energy of the recoiling ions while simultaneously providing electrons that can be captured back into the vacated atomic orbitals. At the right combination of the charge state of the ^{93m}Mo ion and the effective electron kinetic energy, as seen from the reference frame of the recoiling ion, capture can occur, releasing enough energy to match that needed ($\Delta E = 4.85$ keV) to excite the nucleus from the isomer to the intermediate state—that is, NEEC occurs. As described in detail by recent theoretical calculations[16], these NEEC conditions could be fulfilled in practice by capture of an electron at the necessary relative kinetic energy, to within the line width of the capturing atomic vacancy (the NEEC resonance width). The intermediate state in ^{93}Mo that would be populated through NEEC is known to decay (with a half-life of $t_{1/2} = 3.5$ ns) to the ground state through a characteristic sequence of γ-rays at 268 keV, 685 keV and 1,478 keV (Fig. 1). Notably, the 268-keV transition would never be seen in the natural decay of the $21/2^+$ isomer.

The ^{90}Zr + ^{7}Li fusion–evaporation reaction was selected for our experiment, which was performed at the ATLAS facility at Argonne National Laboratory. An 840-MeV ^{90}Zr beam was provided with an average beam intensity of about 6×10^8 ions s^{-1}. The multi-layer target was composed of ^{7}Li supported by a natural carbon (^{nat}C) foil, followed by a gap of about 3 mm and an additional ^{nat}C layer, backed with ^{208}Pb (see Methods for the choice of reaction and target construction). The target was positioned at the centre of the Gammasphere γ-ray spectrometer[17], which, at the time of the experiment, comprised 92 Compton-suppressed, high-purity Ge detectors arranged in 16 rings of constant angle relative to the beam direction. A minimum of three γ-rays within a 2-μs coincidence window was required for events to be recorded to disk, although a narrower, sub-microsecond coincidence constraint was imposed in the offline analysis. We operated the array with a digital data acquisition system (Digital Gammasphere[18]) at average event rates of 40–50 kHz. We collected data for about 62 h in this configuration.

After the fusion of the ^{90}Zr projectiles and the ^{7}Li target nuclei, and the subsequent evaporation of a proton and three neutrons from the compound nuclear system, excited states above the ^{93m}Mo isomer were populated. These excited states depopulated through decay paths that, in some cases, fed the $21/2^+$ isomeric state, such as through the 2,475-keV, $(25/2^+) \rightarrow 21/2^+$ transition (parentheses denote tentative assignments). If a recoiling ^{93}Mo ion is in this isomeric state when the energy–charge resonance conditions are met, NEEC may occur, shifting some of the population of the isomer to the 3.5-ns intermediate state. An observable signature of NEEC would then be the detection of a 2,475-keV γ-ray, which would confirm that the nucleus had reached the ^{93m}Mo state, within the same coincidence window as one or more γ-rays from the decay of the intermediate level. The 2,475-keV

[1]Oak Ridge Associated Universities Fellowship Program, US Army Research Laboratory, Adelphi, Maryland 20783, USA. [2]US Army Research Laboratory, Adelphi, Maryland 20783, USA. [3]Physics Division, Argonne National Laboratory, Argonne, Illinois 60439, USA. [4]Department of Physics, US Naval Academy, Annapolis, Maryland 21402, USA. [5]Department of Nuclear Physics, Research School of Physics and Engineering, Australian National University, Canberra, Australian Capital Territory 0200, Australia. [6]Defense Threat Reduction Agency, Fort Belvoir, Virginia 22060, USA. [7]Faculty of Chemistry, Nicolaus Copernicus University in Toruń, 87-100 Toruń, Poland. [8]National Centre for Nuclear Research, 05-400 Otwock, Poland. [9]Institute of Optics, University of Rochester, Rochester, New York 14627, USA. [10]Flerov Laboratory of Nuclear Reactions, Joint Institute for Nuclear Research, Dubna 141980, Russia. †Present addresses: Department of Physics and Astronomy, University of North Carolina at Chapel Hill, Chapel Hill, North Carolina 27599-3255, USA and Triangle Universities Nuclear Laboratory, Duke University, Durham, North Carolina 27708-2308, USA (R.V.F.J.); Frontier Technology, Inc., Space and Naval Warfare Systems Command, Systems Center Pacific, 49599 Lassing Road, San Diego, California 92152, USA (J.C.M.); Dipartimento di Fisica, Università degli Studi di Milano and INFN sez. Milano, I-20133, Milano, Italy (S.B.).
‡Deceased.

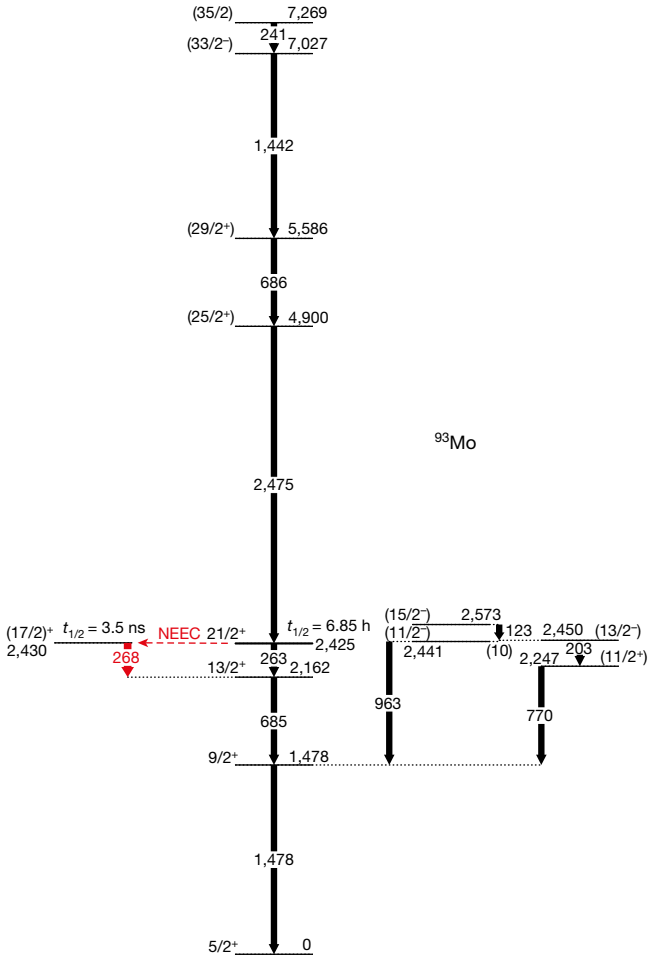

Figure 1 | Relevant part of the ^{93}Mo decay scheme. The energy and the spin and parity quantum numbers (I^{π}, where I denotes the spin and $\pi = +, -$ the parity) are noted for each level, with tentative assignments in parentheses. The half-lives $t_{1/2}$ given for the two isomeric states are from ref. 14. Level and γ-ray energies are from this study and are given in kiloelectronvolts. The 10-keV transition between the $(13/2^-)$ and $(11/2^-)$ states was not observed in this work, but was inferred from the measured coincidence relationships. The NEEC transition from the isomer to the intermediate state is indicated by the dashed red line. The key 268-keV γ-ray is also indicated in red.

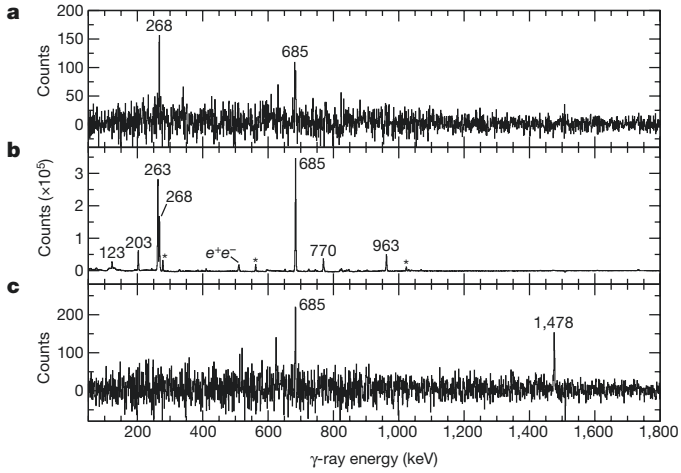

Figure 2 | Spectra demonstrating the signature of NEEC in ^{93}Mo. No correction for the Doppler effect has been applied. **a**, Spectrum obtained with a double gate on the Doppler-shifted 2,475-keV and unshifted 1,478-keV γ-rays. **b**, Spectrum obtained with a single gate on the unshifted 1,478-keV line. **c**, Spectrum obtained with a double gate on the Doppler-shifted 2,475-keV and unshifted 268-keV γ-rays. Peaks of ^{93}Mo shown in Fig. 1 are labelled with their energies in kiloelectronvolts. Additional known ^{93}Mo transitions, not shown in Fig. 1, are marked with asterisks in **b**. The label 'e^+e^-' indicates the 511-keV electron–positron annihilation peak. We note that transitions located above the isomer are too spread out in energy by the Doppler effect to be visible in these spectra.

γ-ray would not ordinarily be found in true coincidence with the 685- or 1,478-keV transitions because of the narrow width (2 μs) of the coincidence window compared to the 6.85-h half-life of the metastable state, nor would it ever be coincident with the 268-keV γ-ray. These coincidences would be possible, however, if some mechanism, such as NEEC, excited the nucleus from the long-lived isomer to the intermediate state.

Each recorded event, consisting of the data for three or more coincident γ-rays, was decomposed into all the constituent subsets of three γ-rays. Energy conditions, or 'gates', were imposed to select two γ-rays out of each set of three, and the counts in a coincidence spectrum were incremented at the energy of the third photon. Background counts, determined by gating on energy ranges near the peaks of interest, were subtracted (see Methods for the gating and background-subtraction procedures, and for the impact of the Doppler effect). A background-subtracted spectrum, produced by a double gate on the 2,475- and 1,478-keV transitions, is presented in Fig. 2a. For comparison, a background-subtracted spectrum, single-gated on just the 1,478-keV γ-ray (that is, the second γ-ray can be at any energy), is also shown in Fig. 2b. In the latter spectrum, the more intense transitions that are coincident with the 1,478-keV γ-ray (see Fig. 1) are clearly visible. With the additional constraint of a gate on 2,475 keV, these lines disappear apart from the 268- and 685-keV peaks (Fig. 2a). The counts in the key 268-keV line are about 7σ above background, where σ is the standard deviation of the counts in the nearby background region (statistical error), or over 3σ when the uncertainty associated with background subtraction is also taken into account (statistical plus systematic errors, as described in Methods). A similar gating procedure on the 2,475- and 268-keV transitions reveals peaks at 685 keV and 1,478 keV, as seen in Fig. 2c. Combined, these spectra demonstrate that the γ-ray sequence 2,475 keV–268 keV–685 keV–1,478 keV occurs in coincidence, which is the expected signature of isomer depletion via NEEC. We note that unlike previous examples of isomer depletion[8,9,19], here the energy of the excitation to the intermediate state is much smaller than that of the isomer itself.

To determine the probability of this excitation, P_{exc}, we summed background-subtracted spectra that were double-gated on the Doppler-shifted lines at 241 keV and 1,442 keV and at 241 keV and 686 keV (see Methods for details). Two versions of this spectrum were generated, as shown in Fig. 3. One had a Doppler correction applied for $v/c = 0.109$ recoils (Fig. 3a), so that the area of the 2,475-keV peak could be determined. The other spectrum had no Doppler correction (Fig. 3b) and was used to obtain the area of the 268-keV peak. As there is no identified decay path from the gating transitions to the 268-keV γ-ray, aside from those involving an excitation such as NEEC, the ratio of the areas of the 268- and 2,475-keV peaks, when corrected for their detection efficiencies, yields the probability that a ^{93m}Mo ion in the long-lived isomeric state (reached via the 2,475-keV transition) subsequently emits a 268-keV γ-ray. An additional, small correction for internal conversion provides the excitation probability, which we determined to be $P_{exc} = 0.010(3)$. The corresponding cross-section, averaged over the full target thickness, is 40 b (see Methods). This is a lower limit, however, as NEEC is a resonant process; the peak cross-section may be much larger. Given that existing cross-section calculations involve very different conditions, such as channelling in a crystal[20,21] or in laser-induced plasmas[22–24], and predict values spanning many orders of magnitude, an in-depth theoretical analysis of our experimental setting is needed. Such analysis is beyond the scope of this study.

At the Heavy Ion Accelerator Facility (HIAF) at the Australian National University (ANU), we explored whether the observed

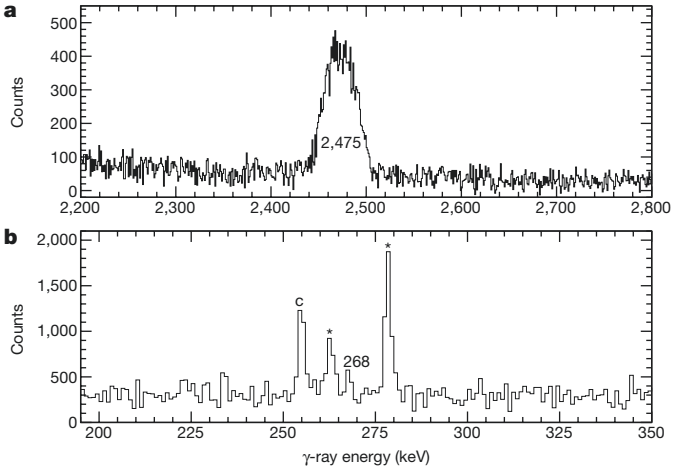

Figure 3 | Spectra used to determine the NEEC probability in ^{93}Mo. The spectra were generated by applying double gates on the Doppler-shifted 241-keV peak and either the 1,442- or 686-keV transitions, placed so as to avoid overlap with the 1,478- and 685-keV ^{93}Mo lines from stopped nuclei at particular angles. **a**, High-energy part of the spectrum, with Doppler correction. **b**, Low-energy part of the same spectrum, but with no Doppler correction. The asterisks mark known transitions in ^{93}Mo; the contaminant labelled with a 'c' comes from ^{95}Ru produced in reactions between the ^{90}Zr beam and the ^{12}C layer of the target.

coincidences could have originated from a different reaction in our experiment. A control reaction between ^{7}Li and ^{90}Zr that created ^{93}Mo recoils with energies that were too small to produce the ionization and electron kinetic energies required for NEEC indeed did not yield the coincident γ-rays that would be a signature of NEEC. Additionally, these γ-rays cannot be attributed to reactions between the ^{90}Zr projectiles and the C or Pb layers in the target (see Methods). We also calculated the probability of ^{93m}Mo being excited to the intermediate state through inelastic scattering (Coulomb and nuclear interaction) at recoil energies above the Coulomb barrier in ^{7}Li and in ^{12}C with the coupled-channel-reaction code FRESCO[25], and through Coulomb excitation at energies below the barrier in ^{208}Pb with the semi-classical coupled-channel Coulomb-excitation code GOSIA[26] using RACHEL[27]. The resulting probabilities are 6×10^{-8}, 2×10^{-6} and 3×10^{-6} in the Li, C and Pb target layers, respectively, all of which are too small to account for the experimental value $P_{exc} = 0.010(3)$ deduced from our data. Thus, the observed coincidences that provide experimental evidence of NEEC do not appear to originate from contaminant reactions or from other well established excitation mechanisms.

Online Content Methods, along with any additional Extended Data display items and Source Data, are available in the online version of the paper; references unique to these sections appear only in the online paper.

Received 26 May; accepted 4 December 2017.

1. Hamilton, J. H. (ed.) *Internal Conversion Processes* 1–13 (Academic Press Inc., 1966).
2. Blatt, J. M. & Weisskopf, V. F. *Theoretical Nuclear Physics* 614–622 (John Wiley & Sons, 1952).
3. Kibédi, T., Burrows, T. W., Trzhaskovskaya, M. B., Davidson, P. M. & Nestor, C. W. Jr. Evaluation of theoretical conversion coefficients using Brlcc. *Nucl. Instrum. Methods A* **589,** 202–229 (2008).
4. Goldanskii, V. I. & Namiot, V. A. On the excitation of isomeric nuclear levels by laser radiation through inverse internal electron conversion. *Phys. Lett. B* **62,** 393–394 (1976).
5. Morel, P., Daugas, J. M., Gosselin, G., Méot, V. & Gogny, D. Nuclear excitation by electronic processes: NEEC and NEET effects. *AIP Conf. Proc.* **769,** 1085–1088 (2005).
6. Pálffy, A., Evers, J. & Keitel, C. H. Isomer triggering via nuclear excitation by electron capture. *Phys. Rev. Lett.* **99,** 172502 (2007).
7. Gosselin, G. & Morel, P. Enhanced nuclear level decay in hot dense plasmas. *Phys. Rev. C* **70,** 064603 (2004).
8. Belic, D. *et al.* Photoactivation of ^{180}Ta^{m} and its implications for the nucleosynthesis of nature's rarest naturally occurring isotope. *Phys. Rev. Lett.* **83,** 5242–5245 (1999).
9. Carroll, J. J. *et al.* Nuclear structure and depletion of nuclear isomers using electron linacs. *AIP Conf. Proc.* **1525,** 586–594 (2013).
10. Roig, O. *et al.* Direct evidence for inelastic neutron "acceleration" by ^{177}Lu^{m}. *Phys. Rev. C* **83,** 064617 (2011).
11. Karamian, S. A. & Carroll, J. J. Cross section for inelastic neutron "acceleration" by ^{178}Hf^{m2}. *Phys. Rev. C* **83,** 024604 (2011).
12. Stefanescu, I. *et al.* Coulomb excitation of ^{68,70}Cu: first use of postaccelerated isomeric beams. *Phys. Rev. Lett.* **98,** 122701 (2007).
13. Karamian, S. A. & Carroll, J. J. Calculated yield of isomer depletion due to NEEC for ^{93m}Mo recoils. *Phys. At. Nucl.* **75,** 1362–1367 (2012).
14. Baglin, C. M. Nuclear data sheets for A=93. *Nucl. Data Sheets* **112,** 1163–1389 (2011).
15. Schiwietz, G. & Grande, P. L. Improved charge-state formulas. *Nucl. Instrum. Methods B* **175–177,** 125–131 (2001).
16. Polasik, M. *et al.* Resonance conditions for ^{93m}Mo isomer depletion via nuclear excitation by electron capture in a beam-based scenario. *Phys. Rev. C* **95,** 034312 (2017).
17. Lee, I.-Y. The Gammasphere. *Nucl. Phys. A* **520,** c641–c655 (1990).
18. Anderson, J. T. *et al.* A digital data acquisition system for the detectors at Gammasphere. In *IEEE Nuclear Science Symposium and Medical Imaging Conference* 1536–1540 (IEEE, 2012).
19. Sethi, J. *et al.* Low-lying states near the $I^{\pi}=6^{+}$ isomer in ^{108}Ag. *J. Phys. G* **43,** 015103 (2016).
20. Kimball, J. C., Bittel, D. & Cue, N. A comment on "nuclear excitation by target electron capture". *Phys. Lett. A* **152,** 367–370 (1991).
21. Yuan, Z.-S. & Kimball, J. C. First-principles calculation of the cross sections for nuclear excitation by electron capture of channeled nuclei. *Phys. Rev. C* **47,** 323–328 (1993).
22. Gunst, J., Litvinov, Y. A., Keitel, C. H. & Pálffy, A. Dominant secondary nuclear photoexcitation with the x-ray free-electron laser. *Phys. Rev. Lett.* **112,** 082501 (2014).
23. Gunst, J., Wu, Y., Kumar, N., Keitel, C. H. & Pálffy, A. Direct and secondary nuclear excitation with x-ray free-electron lasers. *Phys. Plasmas* **22,** 112706 (2015).
24. Wu, Y., Gunst, J., Keitel, C. H. & Pálffy, A. Tailoring laser-generated plasmas for efficient nuclear excitation by electron capture. Preprint at https://arxiv.org/abs/1708.04826 (2017).
25. Thompson, I. J. Coupled reaction channels calculations in nuclear physics. *Comput. Phys. Rep.* **7,** 167–212 (1988).
26. Cline, D. *et al.* GOSIA user manual for simulation and analysis of Coulomb excitation experiments, http://www.pas.rochester.edu/~cline/Gosia/Gosia_Manual_20120510.pdf (2012).
27. Hayes, A. B. & Cline, D. RACHEL graphical interface to GOSIA, https://github.com/adamhayes/Rachel (2017).

Acknowledgements C.J.C. and J.J.C. thank A. D. Ayangeakaa for input on the potential contributions of Coulomb excitations to the background and M. S. Litz and N. R. Pereira for discussions. We also thank J. Rohrer for assistance in setting up the Gammasphere experiment and the ATLAS operations staff for their efforts. This work was initiated under the US Army Research Laboratory (ARL) Director's Research Initiative, award number DRI-FY14-SE-022. Further support was provided by ARL Cooperative Agreements W911NF-12-2-0019 and W911NF-16-2-0034, the US Department of Energy (DOE), Office of Science, Office of Nuclear Physics under contract number DE-AC02-06CH11357, the National Science Foundation under grant number PHY-1203100, the Australian Research Council under grant number FT100100991, and the Polish National Science Centre under grants 2011/01/D/ST2/01286 and 2017/25/B/ST2/00901. M.P., J.R. and A.B.H. received support through Ecopulse, Inc. under ARL contract number W911QX09D0016-0004. This research used resources of Argonne National Laboratory's ATLAS facility, which is a DOE Office of Science User Facility, and of the HIAF at ANU.

Author Contributions C.J.C. led the experimental effort. The experiment was conceptualized by S.A.K. and J.J.C., with the final design provided by C.J.C. and J.J.C. with input from D.J.H. and G.J.L. The targets were prepared by J.P.G. All authors, except S.B., A.B.H. and S.A.K., participated in the experiment. C.J.C. analysed the data, with substantial input from J.J.C. Guidance on the atomic conditions for NEEC was provided by M.P. and J.R. The calculations of inelastic-scattering cross-sections with FRESCO were performed by S.B. and those of Coulomb excitation with GOSIA by A.B.H. We wish to call attention to the role of our late colleague S.A.K., who provided the initial impetus for this work but sadly did not see these results.

Reviewer Information *Nature* thanks O. Kocharovskaya and the other anonymous reviewer(s) for their contribution to the peer review of this work.

METHODS

Reaction choice and target construction. The choice of the beam–target combination for this experiment was based on estimates of the production cross-section of ^{93m}Mo compared to other reaction products and by the need for recoil energies to exceed the NEEC threshold. The cross-sections were calculated using the Monte Carlo fusion–evaporation code PACE4[28] and qualitatively verified experimentally at the HIAF at ANU (C.J.C. *et al.*, manuscript in preparation). A solid target was preferred over He gas[13] to provide a more compact setup inside Gammasphere (a gas cell tens of centimetres in length would have been needed) and to strip traversing ions to a higher charge state[15]. The ^{90}Zr + ^{7}Li combination suitably met these criteria.

The construction and handling of the Li target needed to address several considerations. (1) Li readily oxidizes when exposed to air. (2) Because the decay sequence that is indicative of NEEC involves an intermediate state with $t_{1/2} = 3.5$ ns, enough stopping material must be used to prevent reaction products from moving downstream of the target, out of the view of the Ge detectors. (3) Fusion reactions occurring beyond the first few milligrams per square centimetre of a Li target would produce residues with recoil energies too low to satisfy the NEEC resonance condition. This would yield an incorrect value for the NEEC probability with our method (see Methods section 'Excitation probability and cross-section'), as the 2,475-keV transition to the isomer could be observed for some events with no possibility of NEEC occurring. Thus, stopping all reaction products with a thick Li target (about 15 mg cm^{-2} would be required; http://www.srim.org) is not desirable. (4) Beam ions that traverse the Li layer without reacting can also potentially induce reactions, such as fusion–evaporation or deep-inelastic reactions, with any material placed behind the Li as a stopper. Such reactions, particularly deep-inelastic processes, would yield a large background from dozens of different nuclei, potentially clouding the NEEC signature being sought. This contamination can be considerably reduced by ensuring that the energy of the beam ions incident upon the stopper is reduced to below the Coulomb barrier of the stopping material (ideally, an element with large atomic number Z). (5) For a given ion kinetic energy, a low-Z stopping material is more effective at stripping electrons from the ions down to the inner atomic shells[15], a necessary condition for NEEC. (6) The half-lives of most states above the $21/2^+$ isomer are not known, and some may be comparable to or exceed the stopping time of residues in the target or stopper (of the order of picoseconds). In our approach, observation of a γ-ray directly feeding the isomer was required to ensure that the isomeric state was indeed populated. If the residue has slowed substantially before emission of that γ-ray, the recoil energy may already lie below the NEEC resonance, preventing this process from occurring.

To best address these conflicting requirements, the target was prepared as follows. A 1.55 mg cm^{-2} deposit of ^{nat}Li (abundance of ^{7}Li in ^{nat}Li, about 92%) was evaporated onto a 0.50 mg cm^{-2} ^{nat}C foil. For the stopping material, 33 mg cm^{-2} of ^{208}Pb was placed behind a 4.2 mg cm^{-2} layer of ^{nat}C. The target and stopper were mounted together on a frame with a gap of about 3 mm between the two C layers, as illustrated in Extended Data Fig. 1a. To minimize the risk of oxidation, the target was prepared under vacuum in an evaporator at the ATLAS target laboratory and transported to Gammasphere without breaking the vacuum using the technique described in ref. 29. The target was inserted into the beam path at an angle of 27° from the vertical, increasing the effective thickness of each layer by 12% (Extended Data Fig. 1b). With this target configuration, ^{7}Li(^{90}Zr, $p3n$)^{93}Mo reactions in the first layer can produce ^{93}Mo at high spins and with large recoil energies. The kinetic energy decreases in the remaining Li and thin C layers, before the recoils enter the gap. Then, they drift with constant velocity through vacuum for about 100 ps. Any decays with a cumulative timescale smaller than tens of picoseconds will occur predominantly before the ^{93}Mo ions reach the thicker C layer across the gap; this ensures that the kinetic energies of ^{93}Mo recoils in the isomeric state are still above the NEEC threshold. (A target arrangement with a thicker layer of Li evaporated directly onto a ^{208}Pb backing, with no gap, was used initially. With this target, the line shape of the 2,475-keV γ-ray that feeds the isomer was found to have a sizable narrow component from stopped nuclei. Introducing a gap between the Li target and the stopper eliminates this component, as demonstrated in Extended Data Fig. 2.) The recoils then slow down further in the thicker C layer, where NEEC can occur. Finally, the ^{93}Mo ions come to rest in the ^{208}Pb backing, permitting observation of γ-rays emitted from longer-lived states, such as the 3.5-ns intermediate state. The combined thickness of the C layers was chosen to reduce the ^{90}Zr beam energy to below the Coulomb barrier with ^{208}Pb, so that only a limited number of well known γ-ray transitions produced through Coulomb excitation of ^{90}Zr or ^{208}Pb would be expected.

Spectrum construction and background subtraction. The broad range of level half-lives in the reaction products, combined with the arrangement of a target and stopper separated by a vacuum gap, resulted in complex γ-ray energy spectra: prompt γ-rays were emitted by moving nuclei (average velocity in the gap, $v = 0.109c$), with their energies shifted and peaks broadened owing to the Doppler effect, while slower decays were from stopped nuclei, with no energy shifts or Doppler broadening. Although a correction for the Doppler shift can be applied for a given residue velocity and direction of γ-ray emission, the origin of the γ-rays (from moving or stopped nuclei) is not known on an event-by-event basis. Therefore, it was not possible to apply the appropriate Doppler correction to all γ-rays simultaneously. For the transitions of interest here, the 2,475-keV γ-ray, which lies above the $21/2^+$ isomer, is Doppler shifted, while the 268-, 685- and 1,478-keV γ-rays all lie below the 3.5-ns state and would appear as narrow, unshifted lines.

The anticipated NEEC signature in this experiment would be the observation of a Doppler-shifted 2,475-keV transition in coincidence with the sequence of the 268-, 685- and 1,478-keV γ-rays from stopped nuclei, bypassing the $21/2^+$ isomer. Double-gated, background-subtracted energy spectra were generated as follows. A gate at a particular energy, denoted g in the following, means that the energy of a γ-ray in the detected events fell within designated limits; this gate is composed of the peak of interest (p) atop a smooth background (b), $g = p + b$. A separate energy gate was placed on a nearby, flat part of the spectrum to approximate the background component of the gate. Peak–peak (background-subtracted) coincidence spectra were then constructed for double gates on peaks 1 and 2 using the linear combination

$$p_1p_2 = (g_1 - b_1)(g_2 - b_2) = g_1g_2 - g_1b_2 - b_1g_2 + b_1b_2 \quad (1)$$

where each term on the right-hand side represents the energy bins of a spectrum of the γ-rays in coincidence with those falling within the indicated gate and/or background regions.

Although the γ-ray spectrum is sparser around 2.5 MeV than at lower energies, the Doppler-shifted and broadened 2,475-keV peak spans an energy range of approximately 500 keV when observed over all of the Gammasphere detector angles, overlapping with various lines from stopped nuclei at specific angles. For each ring of detectors, the gate and background windows were selected so as to limit inclusion of such overlapping contaminant lines. The gate on the narrow 1,478-keV line from stopped nuclei was considerably simpler, as the peak is at the same energy in all rings. However, for this gate it was necessary to reject Gammasphere rings 6 to 8 (70° to 81°) because of interference from the Doppler-shifted 1,442-keV transition at those angles. For each transition (and ring), the width of the background window was made the same as that of the corresponding gate. Extended Data Fig. 3 presents the four component spectra of equation (1) for the double gate on the 2,475-keV and 1,478-keV peaks, which was used for Fig. 2a. The energies in these spectra have not been corrected for the Doppler effect in order to show the lines from the stopped nuclei.

Gating in a nearby energy region to approximate the background under a discrete peak is a well established technique[30]. For the 2,475-keV γ-ray, however, the Doppler broadening of the peak at each angle (full-width at half-maximum of tens of kiloelectronvolts, compared to just a few kiloelectronvolts for lines from stopped nuclei) requires that the background gate be placed farther from the peak position than usual. We therefore investigated the effectiveness of our background subtraction method for the 2,475-keV gate. A close inspection of the spectra in Extended Data Fig. 3 reveals that, for the most part, the same peaks appear in each spectrum, with exceptions including the lines at 123, 203, 770 and 963 keV. These four γ-rays are only visible above the background in spectra g_1g_2 and b_1g_2; this indicates that they are all in true, prompt coincidence with the 1,478-keV transition (Fig. 1), but they are coincident with only background Compton-continuum γ-rays in the energy region near 2,475 keV. As these γ-rays should not be in true coincidence with the double gate on 2,475-keV and 1,478-keV (even if NEEC occurred), they are considered background lines. To ensure that the background is suitably subtracted, the spectra $g_1p_2 = g_1g_2 - g_1b_2$ and $b_1p_2 = b_1g_2 - b_1b_2$ were constructed. The peak areas of the four background γ-rays were fitted in both spectra and the ratio k = (area in g_1p_2)/(area in b_1p_2) was calculated for each. The average ratio for the four transitions, k_{ave}, essentially describes the amount of background attributable to Compton γ-rays in the 2,475-keV gate that needs to be subtracted to eliminate these peaks, with the resulting spectrum defined as

$$p_1p_2 = g_1p_2 - k_{ave}b_1p_2 = (g_1g_2 - g_1b_2) - k_{ave}(b_1g_2 - b_1b_2) \quad (2)$$

We find $k_{ave} = 0.99(8)$, which means that equations (1) and (2) are equivalent here. The p_1p_2 spectrum in Fig. 2a, which uses $k_{ave} = 0.99$, demonstrates that the background lines are eliminated whereas the 268- and 685-keV peaks remain. By contrast, eliminating these two lines would require $k = 1.33(7)$ and 1.21(7), respectively; if these peaks originated from true coincidence with the 1,478-keV gate and the Compton background around 2,475 keV, their k values would also be close to $k_{ave} = 0.99$. We used a similar procedure for the double gate on the 2,475- and

268-keV peaks (with a different set of γ-rays in true coincidence with the 268-keV gate) and determined an average ratio $k_{ave} = 1.03(10)$; the central value 1.03 was used for the spectrum in Fig. 2c.

The method of subtracting spectra gated on energies near the peaks of interest eliminates contributions from the smooth Compton background. We estimate from the ^{93}Mo reaction rate that potential contributions of chance coincidences (prompt γ-rays from two independent reactions arriving within the same coincidence window) are small, but would be accommodated by a larger value of k_{ave} to remove the known background lines; the fact that $k_{ave} \approx 1$ suggests that chance coincidences are negligible. A final source of background is the long-lived decay of the $21/2^+$ isomer, which appears at an effectively constant rate in the microsecond-scale coincidence window; however, since the 268-keV transition does not appear in the natural decay of the 6.85-h isomer, these random coincidences do not interfere with the results.

Excitation probability and cross-section. For the background-subtracted spectra presented in Fig. 3, gates were placed on the Doppler-shifted 241-keV peak and on either the 1,442-keV or the 686-keV peaks in each ring of Gammasphere. We took particular care to avoid overlaps at certain angles between these gates and the 1,478- and 685-keV peaks from stopped nuclei. The Doppler-corrected 2,475-keV peak in Fig. 3a does not have a simple Gaussian shape. Rather than fitting the peak by constraining it to a particular shape, we simply determined the area above the background by taking the total number of counts within the energy range of the peak and subtracting the average background derived from the surrounding region of the spectrum. We obtained an area of $A_{2475} = 1.54(3) \times 10^4$ counts. In the spectrum of Fig. 3b, in which no Doppler correction was applied, the 268-keV peak is a narrow line from stopped nuclei that could be fitted (along with the three other peaks of the spectrum) with a Gaussian atop a flat background, yielding an area of $A_{268} = 5.1(16) \times 10^2$ counts. Although we did not measure the absolute detector efficiencies ε_γ, the relative efficiencies of Gammasphere at 2,475 keV and 268 keV (see Methods section 'Energy and efficiency calibrations') are sufficient for determining the ratio $R = \varepsilon_{\gamma,2475}/\varepsilon_{\gamma,268} = 0.28$. By factoring in the intensity of the unobserved internal-conversion branch, which is $\alpha = 0.0355$ times the γ-ray intensity of the 268-keV E2 transition (this branch is negligible for the 2,475-keV transition; see ref. 3 and http://bricc.anu.edu.au), we calculated the excitation probability as $P_{exc} = RA_{268}(1 + \alpha)/A_{2475} = 1.0(3)\%$ for ^{93m}Mo nuclei traversing the C target.

As a comparison, in ref. 13 a probability of 0.01% is calculated for NEEC in ^{93}Mo, but it is stated that this value could be much higher because certain parameters were not very well known. Although the experimental conditions proposed in that work for the observation of NEEC are similar to those used in our experiment, the excitation probabilities cannot be directly compared because the predicted value is dependent upon NEEC occurring in a specific length of helium gas[13]. Similarly, this sensitivity of the excitation probability to the experimental conditions prevents a reliable comparison of our measurement with other existing theoretical predictions.

The excitation probability P_{exc} can be expressed in terms of a cross-section $\sigma_{exc} = N_{exc}/(N_{proj}n)$ where N_{exc} and N_{proj} are the numbers of excitations and projectiles, respectively, and n is the number of target atoms per unit area. The ratio N_{exc}/N_{proj} here is equivalent to P_{exc}, while n can be written as $n = \rho N_A/A_t$, where ρ is the target surface density, A_t is the mass per mole of the target and N_A is the Avogadro constant. The full thickness of C in the target had $\rho \approx 5$ mg cm^{-2} and the average cross-section across this thickness would be 40 b. This implies a much larger peak cross-section for the resonance, but it is worth noting that rather large values have been suggested for other scenarios[31].

Alternative reactions and excitation mechanisms. The same reaction that was examined in this work was investigated at ANU with the beam and target nuclei interchanged and at a similar centre-of-mass energy (C.J.C. *et al.*, manuscript in preparation). Both reactions are expected to populate the same set of excited states. However, in normal kinematics, with a light beam (^{7}Li) on a heavy target (^{90}Zr), the kinetic energy of the resulting ^{93}Mo recoil would be too low for NEEC to occur. The analysis of that dataset demonstrated that under those conditions the 2,475-keV γ-ray was not coincident with either the 268-keV or the 1,478-keV transitions in ^{93}Mo or in any other nuclide produced in the ^{7}Li + ^{90}Zr reaction. Similarly, reactions between the ^{90}Zr projectiles and the C in our layered target were ruled out as the origin of the observed coincidences by examining the ^{12}C + ^{90}Zr reaction (C.J.C. *et al.*, manuscript in preparation). Thus, the observed γ-ray sequence 2,475 keV–268 keV–685 keV–1,478 keV did not originate from contaminant fusion–evaporation reactions involving either Li or C. (As noted earlier, reactions between ^{90}Zr and the Pb stopper are expected to yield only a couple of γ-rays with well known energies following Coulomb excitation.) Although these measurements were performed at a different facility from the NEEC experiment at ATLAS, the detector array at ANU is sufficiently sensitive to detect such coincidences had they existed in normal kinematics, given the excitation probability deduced from the ATLAS experiment.

Coulomb excitation and inelastic scattering of ^{93m}Mo are possible alternative mechanisms by which the nucleus could be excited from the isomer to the intermediate state (as was observed for ^{68m}Cu in ref. 12). We used the codes GOSIA[26] and RACHEL[27] to calculate the expected yield of 268-keV γ-rays from the intermediate state as a fraction of the total number of ^{93m}Mo recoils incident on ^{208}Pb. GOSIA requires electromagnetic transition strengths as input. Although few transition strengths in ^{93}Mo have been experimentally determined, several could be estimated from the analogous transitions in ^{92}Mo owing to the close structural similarity of these two isotopes[32]. For the 4.85(9)-keV, $21/2^+ \rightarrow (17/2)^+$ E2 excitation[14], a reduced transition strength of $B(E2) = 72e^2$ fm^4, where e is the charge of the electron, can be obtained from the shell-model estimate of ref. 33, which is about two times larger than the strength[34] $B(E2; 8^+ \rightarrow 6^+)$ of the analogous transition measured in ^{92}Mo. Weaker (or unobserved) transitions between other pairs of states were assumed to have smaller transition rates than those noted above. With these assumptions, we determine the probability of exciting the isomer to the intermediate state via Coulomb excitation in ^{208}Pb to be approximately 3×10^{-6}. This probability is dominated by the direct transition between the two states, with minimal impact from multistep excitations involving other states, and repeating the calculation with a drastically simplified level scheme (containing only these two states plus those below the isomer) yields comparable results. Additionally, even by increasing the strength $B(E2; 21/2^+ \rightarrow (17/2)^+)$ by 100 times, which exceeds the recommended upper limit[35], the resulting probability of 2×10^{-4} is still much lower than the experimental $P_{exc} = 0.010(3)$.

We also used FRESCO[25] to calculate the expected cross-sections for the excitation of ^{93m}Mo to the intermediate state via above-barrier inelastic scattering in Li and in C. Using the GOSIA findings as a starting point, a simplified level scheme with only direct excitation of the intermediate state was assumed to be sufficient. The reduced transition strength of $72e^2$ fm^4 was again used. Extended Data Fig. 4 shows the cross-sections as a function of ^{93}Mo recoil energy in both target materials, as calculated by FRESCO. Taking the average cross-section in each medium separately, the corresponding probabilities for the $21/2^+ \rightarrow (17/2)^+$ excitation are 6×10^{-8} in Li, assuming ^{93}Mo production at the centre of the target, and 2×10^{-6} over the full thickness of C.

We note that GOSIA and FRESCO are well established reaction codes validated by substantial experimental data. While various NEEC models have existed for several decades, there have been no prior non-null experimental results to test their reliability.

Energy and efficiency calibrations. We performed both energy and relative-efficiency calibrations of the Gammasphere Ge detectors using ^{152}Eu and ^{56}Co calibration sources. Each source was positioned in the target location, at the centre of Gammasphere. The energies and intensities of the strongest γ-rays that are emitted after the decay of these nuclides, which span from 122 keV to 1,408 keV (^{152}Eu) and 847 keV to 3,451 keV (^{56}Co), are well known. We fitted the peak centroids and areas and compared them with these known energies and intensities, respectively, using the RadWare suite of analysis codes (http://radware.phy.ornl.gov). The data from both sources were combined for the energy calibration and were simultaneously fitted with a second-order polynomial. The detection efficiencies of the Ge detectors had a more complex energy dependence[36] and the two sources were treated separately, as their absolute activities were not precisely known. We performed a preliminary fit of the ^{152}Eu lines and then normalized the ^{56}Co relative efficiencies to those of ^{152}Eu in the region where the energies for the two sources overlap to obtain an efficiency curve for the full 0.1–3.4-MeV energy range. This procedure provided relative efficiencies, but these are sufficient because our analyses use only efficiency ratios.

Uncertainties. The uncertainty on the counts in each energy bin of a spectrum double-gated on a peak or the background was taken to be the square root of the number of counts in that energy bin. For a background-subtracted spectrum formed by a linear combination of the component spectra (equations (1) or (2)), the uncertainty was that of the individual components added in quadrature. These uncertainties were used as statistical weights for each energy bin in the fits to the peak areas.

The systematic errors associated with the spectra in Fig. 2a, c were taken to be the uncertainties in k_{ave}, as determined from the known background γ-rays in each spectrum. We could then define the total uncertainty σ as the statistical and systematic errors added in quadrature. For example, the weighted average of $k = 1.33(7)$ and 1.21(7) for the 268- and 685-keV peaks in the double gate on the 2,475- and 1,478-keV peaks (Fig. 2a) is $k_{NEEC} = 1.27$ with statistical uncertainty 0.05, while the systematic uncertainty on $k_{ave} = 0.99$ is 0.08. The total uncertainty is $\sigma = (0.05^2 + 0.08^2)^{1/2} = 0.09$, and thus the peaks from NEEC are $k_{NEEC} - k_{ave} = 0.28 = 3\sigma$ above background (compared to a level of about 7σ from

a purely statistical uncertainty). A similar analysis for the double gate on the 2,475- and 268-keV peaks (Fig. 2c) also produces a 3σ result.

Code and data availability. The 7-TB dataset generated and analysed during this study is available from the corresponding author on reasonable request. The codes used in the analysis, aside from those cited in the references, are also available.

28. Tarasov, O. B. & Bazin, D. Development of the program LISE: application to fusion-evaporation. *Nucl. Instrum. Methods B* **204,** 174–178 (2003).
29. McCutchan, E. A., Lister, C. J. & Greene, J. P. A target vacuum interlock system for Gammasphere. *Nucl. Instrum. Methods A* **607,** 564–567 (2009).
30. Radford, D. C. Background subtraction from in-beam HPGe coincidence data sets. *Nucl. Instrum. Methods A* **361,** 306–316 (1995).
31. Pálffy, A., Harman, Z. & Scheid, W. Quantum interference between nuclear excitation by electron capture and radiative recombination. *Phys. Rev. A* **75,** 012709 (2007).
32. Fukuchi, T. *et al.* High-spin isomer in ^{93}Mo. *Eur. Phys. J. A* **24,** 249–257 (2005).
33. Hasegawa, M., Sun, Y., Tazaki, S., Kaneko, K. & Mizusaki, T. Characteristics of the $21/2^+$ isomer in ^{93}Mo: toward the possibility of enhanced nuclear isomer decay. *Phys. Lett. B* **696,** 197–200 (2011).
34. Baglin, C. M. Nuclear data sheets for A=92. *Nucl. Data Sheets* **113,** 2187–2389 (2012).
35. Firestone, R. B. *et al.* (eds) *Table of Isotopes* 8th edn, Vol. II (John Wiley & Sons, 1996).
36. Radford, D. C. ESCL8R and LEVIT8R: software for interactive graphical analysis of HPGe coincidence data sets. *Nucl. Instrum. Methods A* **361,** 297–305 (1995).

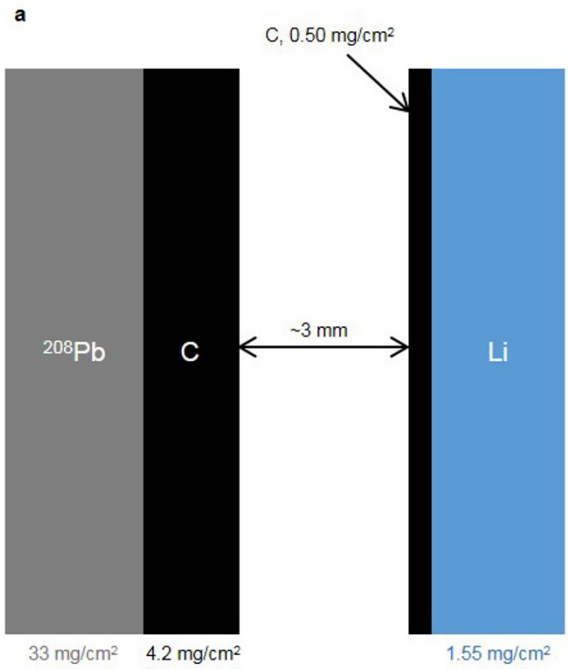

Extended Data Figure 1 | Configuration of the target used in the experiment. a, Schematic of the target construction showing the layers in which ^{93}Mo production occurs (Li), NEEC can occur (C) and the backing that stops all recoils (^{208}Pb), in addition to the important gap of about 3 mm that is needed to accommodate the effective half-life for the decay of the 4,900-keV level. Relative dimensions are not to scale. The beam is incident on the Li surface. **b**, Photograph of the target positioned inside the Gammasphere target chamber. The beam enters from the lower right side and is parallel to the double rods shown in the upper left part of the photograph.

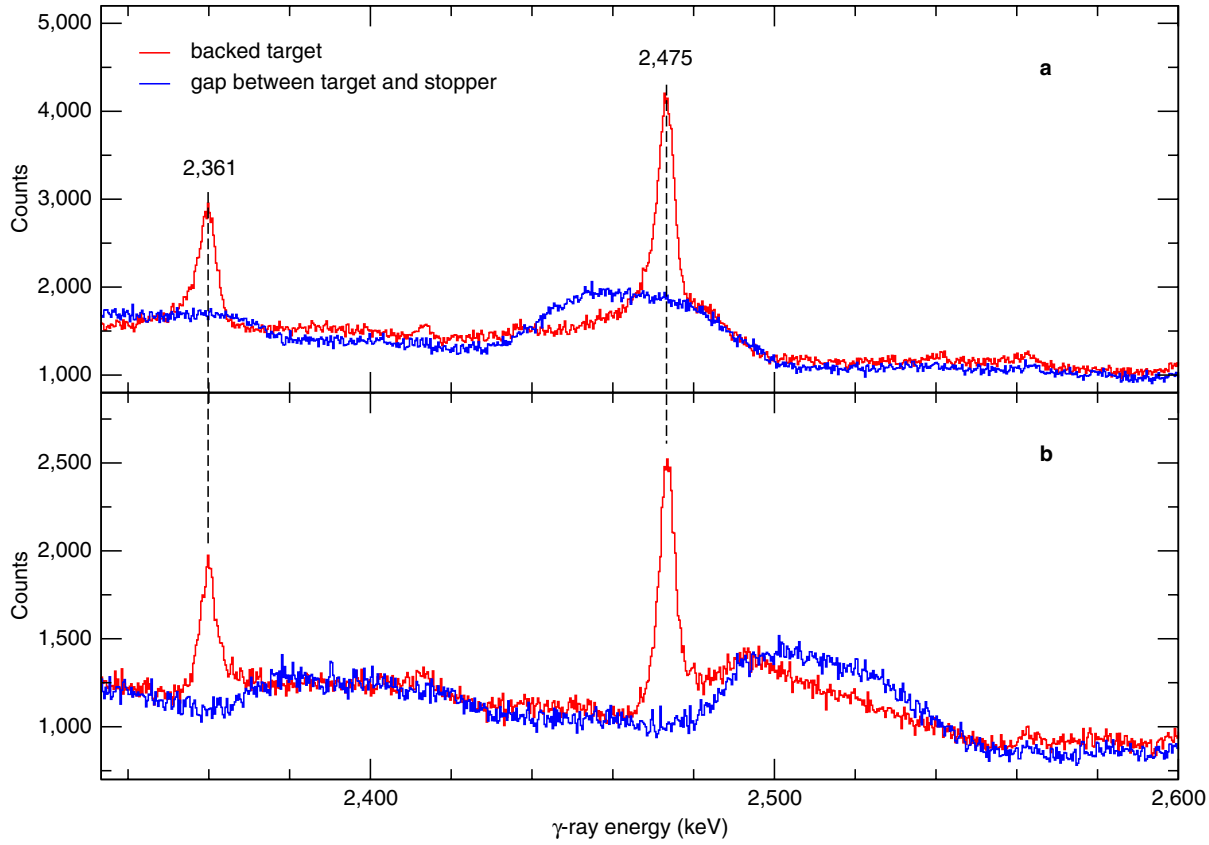

Extended Data Figure 2 | Spectra showing the line shape of the 2,475-keV transition in ^{93}Mo. a, **b**, The spectra are from the detectors in ring 9 of Gammasphere at 90° (**a**) and ring 7 at 79° (**b**). The spectra in red were recorded while using a Li target backed with ^{208}Pb and with no gap in between. The blue spectra were obtained with a modified target configuration with a gap of about 3 mm. The 2,361-keV peak corresponds to a transition in ^{92}Mo that lies below a level with a half-life of $t_{1/2} = 35$ ps. The similar line shapes of these two transitions support the estimate of a delay of tens of picoseconds in the 2,475-keV emission and therefore the rationale for the final target construction.

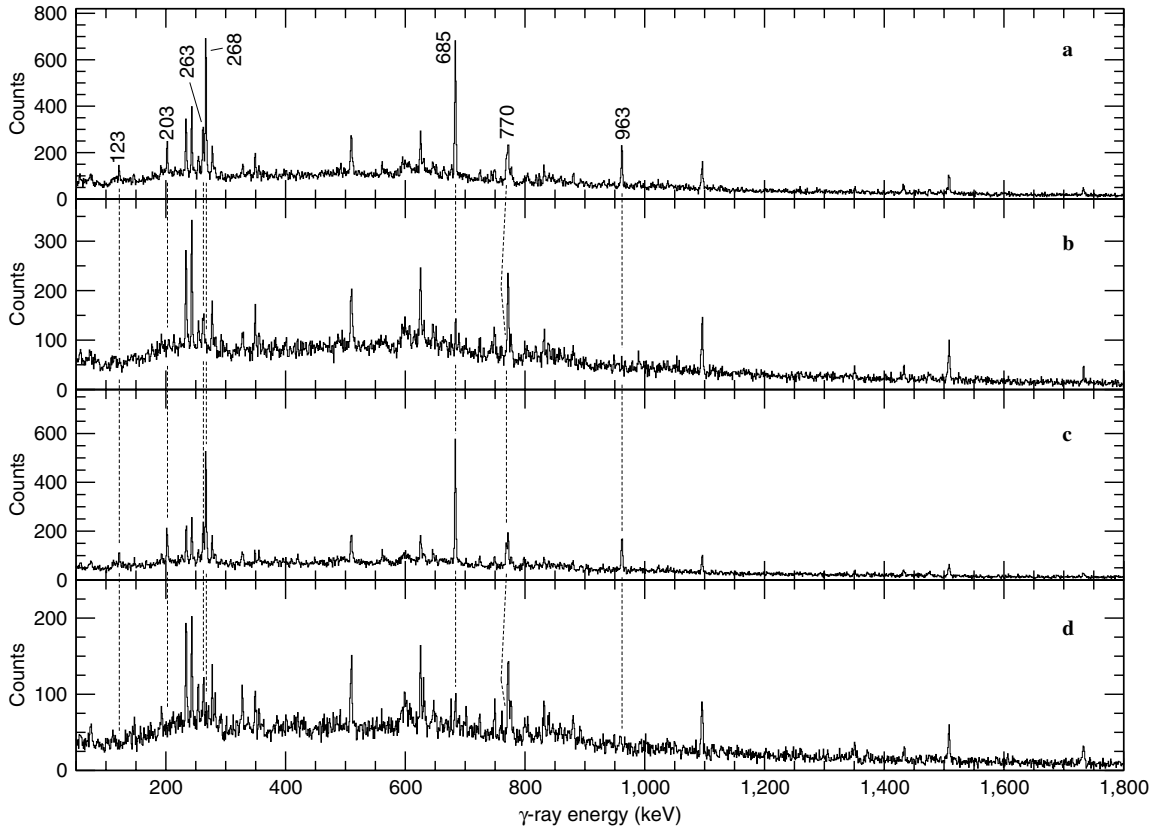

Extended Data Figure 3 | Spectra used to determine background contributions. Component spectra for the double gate on the Doppler-shifted 2,475-keV γ-ray (1) and the unshifted 1,478-keV γ-ray (2), where gates on the peak and background regions are denoted as '*g*' and '*b*', respectively (see text). **a**, g_1g_2. **b**, g_1b_2. **c**, b_1g_2. **d**, b_1b_2. Only those γ-rays in ^{93}Mo relevant to the discussion are labelled, with the dashed lines marking their energies. We note that the 770-keV peak in **a** is a multiplet with the 773- and 777-keV transitions in ^{92}Mo and ^{97}Ru, respectively; only the last two peaks appear in **b** and **d**.

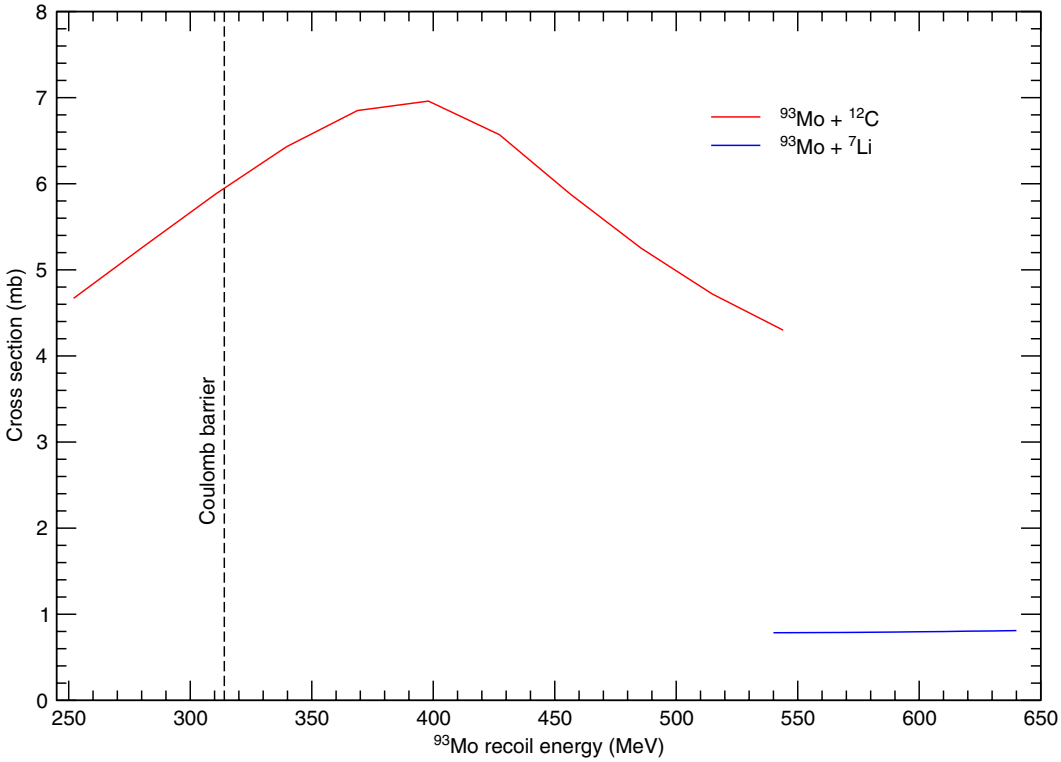

Extended Data Figure 4 | Calculations of possible competing processes. The inelastic-scattering cross-sections for exciting ^{93m}Mo to the intermediate state, calculated with the code FRESCO, are plotted versus the energy of recoiling ^{93}Mo ions traversing the ^{7}Li (blue) and ^{12}C (red) target layers. The initial energy is the average recoil energy corresponding to ^{93}Mo production at the centre of the Li target.